

Influence of Cr growth on exchange coupling in Fe/Cr/Fe(100)

D. T. Pierce, Joseph A. Stroschio, J. Unguris, and R. J. Celotta

Electron Physics Group, National Institute of Standards and Technology, Gaithersburg, Maryland 20899

(Received 19 January 1994)

Scanning electron microscopy with polarization-analysis (SEMPA) measurements of the dependence of the oscillations of the exchange coupling in Fe/Cr/Fe(100) structures on the Cr growth temperature are correlated with the thickness fluctuations in Cr films measured by scanning tunneling microscopy (STM) at similar growth temperatures. Layer-by-layer growth was observed by STM for Cr deposition on very flat Fe(100) whiskers at deposition temperatures $\geq 300^\circ\text{C}$. The SEMPA measurements of the magnetization of the Fe overlayer as a function of Cr spacer-layer thickness at this temperature could be simulated well by oscillatory coupling with periods $2.105 \pm 0.005d$ and $12 \pm 1d$, where d is the layer spacing. Rougher Cr growth, limited by diffusion kinetics, occurs at lower growth temperatures giving a distribution of thicknesses in the growth front as determined by STM. We modeled the Fe magnetization for lower-temperature Cr growth by assuming that the exchange coupling at each discrete Cr thickness is the same as found for layer-by-layer growth. The total coupling at each average Cr spacer-layer thickness was determined by adding the weighted contribution to the coupling from each Cr layer thickness contributing to the average thickness. Thus, by taking into account the thickness fluctuations in the Cr spacer layer as determined by STM, very good agreement was obtained between the model and the SEMPA measurement of the Fe overlayer magnetization for Cr growth at lower temperatures without including other consequences of roughness at the interface, such as the breakdown of translational invariance. Important characteristic length scales and the role of biquadratic coupling in the SEMPA measurements are addressed.

I. INTRODUCTION

The exchange coupling between two magnetic layers separated by a nonmagnetic layer has been an increasingly active area of investigation, due in part to the "giant magnetoresistance" or "spin-valve effect" seen^{1,2} in coupled layers, and its potential importance to magnetic sensor technology. Some years ago it was found³ that two layers of Fe, each several monolayers⁴ thick, coupled antiferromagnetically when separated by a particular thickness of Cr (that is, with the magnetization in one Fe layer antiparallel to that in the other Fe layer). Subsequently, it was found⁵ that if the thickness of the Cr layer is varied, there is an oscillation between ferromagnetic and antiferromagnetic coupling of the Fe layers. This oscillatory exchange coupling has now been found⁶ for numerous magnetic materials and a variety of nonmagnetic metal spacer layers. The electronic structure of the spacer layer material is now understood⁷ to determine the periods of oscillation.

Key to our understanding of the exchange coupling of the layers has been the observation of multiple oscillatory coupling periods, and the precise determination of these periods to permit correlation with the spacer-layer electronic structure. Using scanning electron microscopy with polarization analysis (SEMPA) to investigate the coupling of epitaxially grown Fe/Cr/Fe(100) trilayers, it was found that in addition to the long-period coupling that had been previously observed in sputtered multilayer structures, a short period of approximately two atomic layers was present and could even be dominant depending on the sample preparation conditions.⁸ The critical ex-

perimental parameter was the temperature of the Fe(100) substrate during Cr evaporation. Reflection high-energy electron-diffraction (RHEED) measurements of these films indicated that temperature affected the Cr film growth. In this paper we present scanning tunneling microscopy (STM) measurements of the growth of Cr on Fe(100) under conditions similar to the sample preparation conditions of the SEMPA measurements, and obtain a detailed determination of the surface morphology. We show how the roughness of the Cr growth front translates into fluctuations in the thickness of the Cr spacer layer and provides an explanation for the SEMPA observations that the oscillations in the exchange coupling depend on the Cr growth temperature. These results for the prototype Fe/Cr/Fe system, which show the sensitivity of the exchange coupling to the physical structure, reveal a likely source for many of the numerous discrepancies in the coupling measurements of a variety of systems reported in the literature.

II. SEMPA MEASUREMENTS OF MAGNETIC COUPLING

The SEMPA measurements were made on Fe/Cr/Fe(100) structures described previously,⁸ in which the Cr was deposited in a "wedge-shaped" layer of linearly increasing thickness on the nearly perfect single crystal Fe whisker substrate held at a designated temperature. A thin film of Fe, 5–10 monolayers thick, was then evaporated on the Cr at room temperature. A schematic of this sample structure is shown in Fig. 1. The wedge geometry has the advantages that it allows measurements

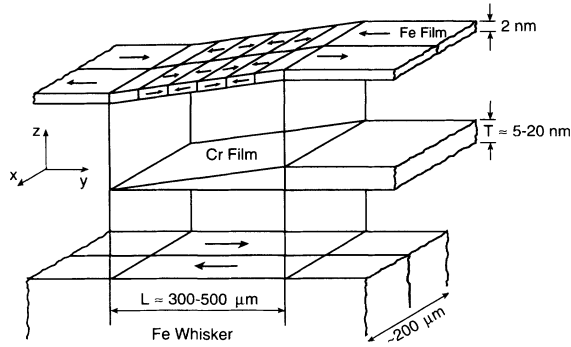


FIG. 1. A schematic exploded view of the Fe/Cr/Fe(100) sample structure showing the Fe(100) single-crystal whisker substrate, the Cr wedge, and the Fe overlayer. The arrows show the magnetization direction in each domain. The z scale is expanded approximately 5000 times.

at many different thicknesses, with a reproducibility in relative thickness that could not be obtained from many individual sandwiches, and that films of all thickness are prepared under identical conditions. Also, in the case of high-temperature Cr growth, the absolute number of monolayers all along the wedge can be determined very precisely. The thickness scale is calibrated using RHEED intensity oscillations measured as the SEM beam is scanned along the wedge after growth. These "spatial" RHEED intensity oscillations can be registered with SEMPA images by aligning defects. This allows a determination of the Cr thickness to ± 0.1 monolayer at any point in the image in the case of high-temperature growth.⁸⁻¹⁰ The SEMPA magnetization images of the Fe overlayer are obtained by measuring the spin polarization of the secondary electrons generated by the highly focused SEM beam as described elsewhere.^{11,12} It is convenient to grow the Cr wedge on a portion of the Fe whisker where there are two domains, as shown in Fig. 1, in order to eliminate any zero offsets due to instrumental asymmetries. For simplicity, the magnetization images presented in this paper will be from one domain.

The strong dependence of the exchange coupling on the growth temperature of the Cr is shown in Fig. 2, which displays SEMPA images of magnetization for cases in which the Cr was evaporated onto the Fe substrate held at 30, 200, and 350 °C, respectively. The images show the magnetization component along the whisker, M_y , in the coordinates of Fig. 1. The underlying Fe whisker magnetization is in the direction of increasing Cr thickness, i.e., in the positive M_y direction. The magnetization of the Fe overlayer is initially ferromagnetically coupled with its magnetization parallel to the substrate (white regions in the figure) at the left side or thinnest part of the wedge, and then changes to antiferromagnetic coupling (black regions) and back in an oscillatory manner as the Cr thickness increases. We have previously reported magnetization images at room temperature⁸ and high temperature⁹ which showed well-defined oscillatory coupling out to 60 and 75 monolayers, respectively. In Fig. 2, we show only the coupling out to a maximum

Cr layer thickness of 40 monolayers, which is at the right side of each image, corresponding to the data available at the intermediate temperature. The Cr thickness increases from 0 to 40 monolayers over a distance of approximately 0.4 mm on the Fe whisker for the samples displayed in Fig. 2.

III. STM MEASUREMENTS OF Cr GROWTH

The STM measurements were first used to characterize the clean Fe(100) whisker surface used as a substrate for the wedge sample structures.¹³ The surface was prepared by sputtering initially at room temperature followed by

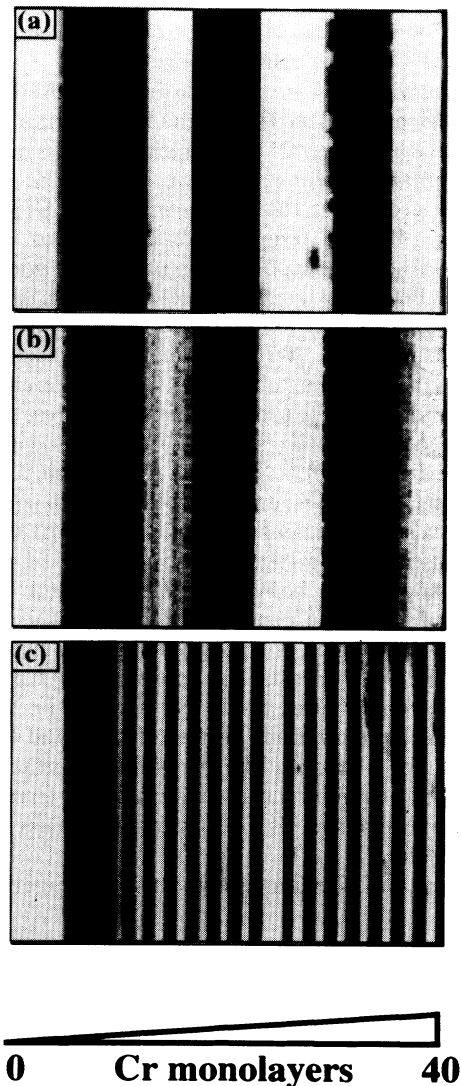


FIG. 2. SEMPA magnetization images of the Fe overlayer coupled through Cr spacer layers grown on Fe substrate temperatures of (a) 30, (b) 200, and (c) 350 °C, respectively. The Cr spacer layer increases in thickness from 0 to 40 monolayers, as indicated, from the left to the right of the images. The magnetization of the Fe overlayer is parallel (ferromagnetically coupled) to the substrate in the white regions, and antiparallel (antiferromagnetically coupled) in the black regions.

sputtering at 750°C to obtain a clean well-ordered surface.¹⁴ The STM images were obtained on a custom STM system described previously.¹⁵ It was further equipped with evaporators for epitaxial growth of Cr and Fe and RHEED to monitor the growth. A large area, 3.5 μm wide, STM image typical of the clean Fe whisker surface is shown in Fig. 3. There are three single-atom high steps visible. The variation in gray level corresponds linearly to the height variation with the lowest level in the image being darkest. What is remarkable is the large flat terraces with approximately one step each micrometer. This corresponds to an alignment of the (100) surface to better than 0.01°, which is much better alignment than is obtained in the conventional preparation of metal crystals. Further, there is no damage due to surface polishing. The lattice mismatch between Cr and Fe is only 0.6% vertically as well as laterally, so there is little disturbance in the Cr layers caused by the step.

The striking variation in the nature of the oscillatory exchange coupling as a function of the temperature of the Fe(100) substrate during Cr evaporation can be seen in Fig. 2. A similarly striking variation is also seen in the nature of the growth of the Cr shown in the STM images¹⁶ of Fig. 4. The temperature dependence of Cr growth was studied by evaporating a particular thickness of Cr on the Fe(100) whisker surface held at a specific temperature, and then cooling to room temperature for the STM measurements. With this method, "snapshots" of the growth can be obtained¹⁷ for different Cr thicknesses and different substrate temperatures, as we have illustrated in extensive studies of the homoepitaxial growth of Fe on Fe(100).^{13,18} When a Cr atom reaches the Fe surface, it diffuses until it collides with another atom to form a stable nucleus for island growth or until it reaches an existing island edge and is incorporated. Thus there is a competition between nucleation and island growth depending on the deposition rate and on the surface diffusion rate, which is strongly temperature dependent. From the STM measurements we obtain a picture of the growth front; that is, the height distribution of the surface. Because the interface between the Cr and the Fe whisker substrate is smooth like the whisker surface, the roughness in the Cr film surface within a flat terrace of the Fe substrate corresponds directly to a thickness variation of the Cr film.

A STM image of the film grown at low temperature,

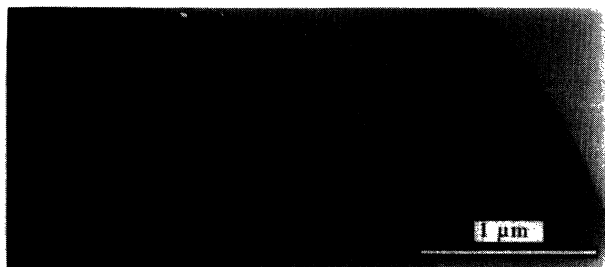


FIG. 3. A $1.6 \times 3.5\text{-}\mu\text{m}$ STM image of the clean Fe(100) whisker showing the typical step density of approximately one per micrometer. Higher regions of the surface are indicated by lighter gray levels.

$50 \pm 20^\circ\text{C}$, with an average thickness of five monolayers, is shown in Fig. 4(a). The variation in gray levels visible in the image correspond to regions of Cr in the growth front that are 3–7 monolayers thick. In Fig. 5, we plot the amount of each thickness exposed, $\Theta_n - \Theta_{n+1}$, that is, that can be seen looking down on the surface—where Θ_n is the coverage of the n th layer. Empirically, we find that the fraction of each thickness exposed can be approximated by a Gaussian where the standard deviation σ is a measure of the interface width. It is equal to the root-mean-square height variation or rms roughness h_{rms} given by

$$\sigma = h_{\text{rms}} = \langle (h - \langle h \rangle)^2 \rangle^{1/2}. \quad (1)$$

For the Cr growth at 50°C, the rms roughness is 0.86 monolayers (0.124 nm). Recall that $\pm 2\sigma$ includes 95% of the height fluctuations. The width of the growth front

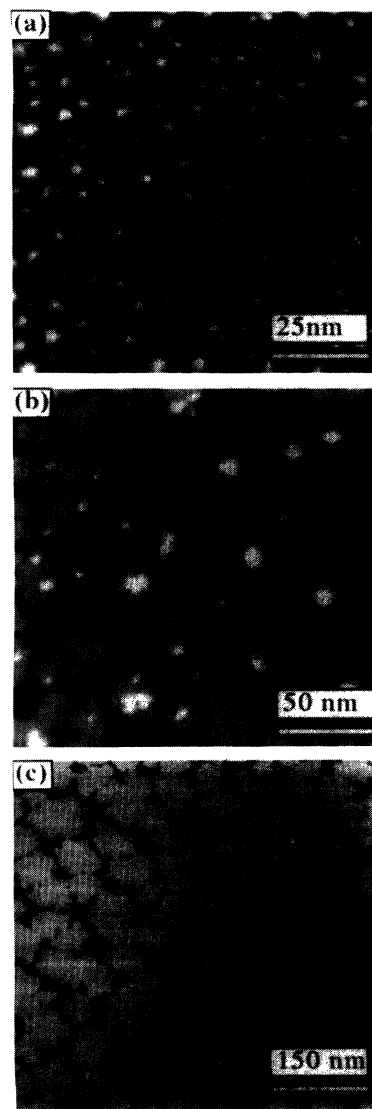


FIG. 4. STM images show the growth of Cr on the Fe(100) whisker substrate held at (a) 50, (b) 215, and (c) 300°C. The images are 100×100 , 200×200 , and 600×600 nm, respectively.

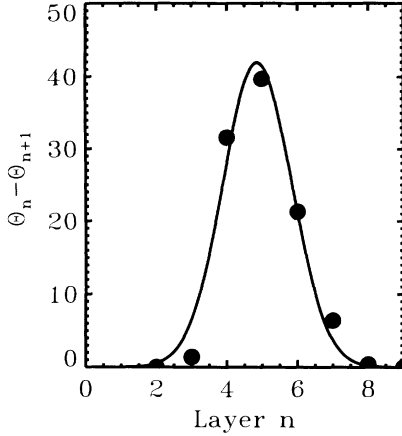


FIG. 5. The percent coverage of each thickness exposed in the growth front of a Cr film, with an average thickness of five monolayers, grown on Fe(100) held at 50 °C is seen to be fit well by a Gaussian with σ the rms roughness.

for Cr grown at 50 °C is thus 3.4 monolayers using 4σ as the measure of the height fluctuations. At temperatures such that the diffusion takes place slowly, the roughness is expected to increase with thickness t according to the power law¹⁹

$$\sigma = Ct^\beta. \quad (2)$$

In the case of the growth of Fe on Fe(100), which we have studied^{13,18} in great detail, we found that for up to 20 monolayers the rms roughness could be described well by Eq. (2) with $\beta = 0.457 \pm 0.087$.⁴

The surface of a Cr film grown at 215 ± 20 °C with an average thickness of 4.65 monolayers is shown in the STM image of Fig. 4(b). It has a rms roughness of 0.47 monolayers (0.068 nm). The four gray levels correspond to thicknesses of 3–6 monolayers which are visible in the image. The island size, of order 20 nm, is approximately 20 times larger than for the low-temperature growth. There is a qualitative difference in the growth of Cr on the Fe whisker at the higher temperature of 300 ± 20 °C, as seen in Fig. 4(c), which shows a film with an average thickness of 3.7 monolayers. At this temperature, the incident atoms diffuse readily and large islands are obtained which grow to complete one atom layer before the next atom layer begins; that is, the growth is truly in the “layer-by-layer” mode. This case of true layer-by-layer growth has characteristic cusplike RHEED intensity oscillations which persist with little decay in the intensity maxima.¹⁶

IV. MODELING THE EXCHANGE COUPLING

In order to understand how the differences in Cr growth affect the Fe magnetization observed in the SEMPA images, we begin by modeling the interaction of two perfect Fe layers, and show that it successfully simulates the SEMPA data when the Cr grows in the layer-by-layer mode. The interaction J_1 as a function of the spacer layer thickness t asymptotically takes the form,^{20,21}

$$J_1(t) = \sum_s F_s(t) \sin(k_s t + \Phi_s), \quad (3)$$

where $F_s(t)$ is a slowly varying envelope function, k_s is a Fermi-surface spanning vector, and Φ_s gives the phase. $F_s(t)$ includes factors that depend on the geometry of the Fermi surface and on the spin-polarized reflection amplitudes for electron states at the extremum of the Fermi surface. At zero temperature,²¹ for a simple extremum with no nesting, the thickness dependence of $F_s(t)$ is just $1/t^2$; for partial nesting it is $1/t^{3/2}$, and for complete nesting it is $1/t$. For finite temperatures, there is also an exponential decay of the coupling with a decay length that depends on the geometry of the Fermi surface and the temperature.²¹ Although Eq. (3) is strictly speaking the asymptotic form of the interaction for well-separated magnetic layers, it often holds very well even for thicknesses as small as one oscillation period.²⁰

The magnetization direction of the top Fe film depends on J_1 ; that is, the film couples ferromagnetically or antiferromagnetically to the underlying Fe whisker depending on whether J_1 is positive or negative. The SEMPA magnetization image shows the direction of this magnetization. It does not give a direct measurement of the strength of J_1 , but it allows a precise determination of the Cr thickness where J_1 changes sign. We determine the coupling periodicities from such data. For example, consider a magnetization image such as that of Fig. 2(c) for the case of the layer-by-layer Cr growth. The value of the magnetization component in the direction of increasing Cr thickness is plotted in Fig. 6(c). These data have two frequency components, with the short period component dominating. The square-wave nature of the profile prevents extracting precise periods $L = 2\pi/k_s$ by a simple Fourier transformation, but we can use Fourier analysis to obtain starting values for use in an accurate fitting procedure. We model the interaction by a sum of two sine waves,

$$J_m(n) = (1/nd)A \sin(2\pi nd/L_A + \Phi_A) + (1/n^2 d^2)B \sin(2\pi nd/L_B + \Phi_B), \quad (4)$$

where the zero temperature thickness dependence has been factored out and the remaining part of $F_s(t)$ absorbed in the relative amplitudes A and B . The $1/t$ dependence of the first term in Eq. (4) is appropriate for the special case of the short-period coupling, which arises from the nearly perfect nesting of parts of the Cr Fermi surface centered at Γ and H .²¹ This same strong nesting is the origin of the spin-density-wave antiferromagnetism in Cr. The model interaction $J_m(n)$ is plotted as the solid circles in Fig. 6(c); it only has values at each thickness nd corresponding to a discrete number of monolayers n , each of thickness d . J_m is arbitrarily normalized in Fig. 6 to J^* , the value of $J_m(n)$ for one monolayer; that is, for $n=1$ in Eq. (4). In a real film, as seen in the STM images of Fig. 4, each average Cr film thickness can consist of multiple regions, each with a different number of monolayers. The strength of the effective interaction at any average thickness t is the sum of the interactions $J_m(n)$ weighted by the fraction of the area at that average thickness having n monolayers.

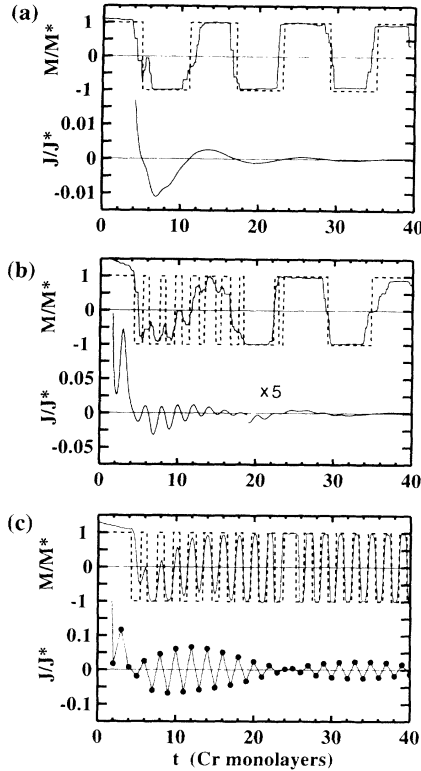


FIG. 6. Profiles M/M^* of the normalized (see text) magnetization M_y from the SEMPA images of Fig. 2 are shown as solid lines in the upper parts of each panel corresponding to Cr growth at Fe substrate temperatures of (a) 30, (b) 200, and (c) 350°C, respectively. The dashed line is the model magnetization calculated as described in the text. The solid line J/J^* in the lower part of each panel is the normalized (see text) interaction $J_m(t)$ at the average thickness t calculated from the inter-layer exchange coupling $J_m(n)$, the coupling at each discrete thickness nd (shown by solid circles), taking account of the thickness fluctuations in the Cr growth.

In the case of layer-by-layer growth, if a fraction α of atom layer $n+1$ grows, then $1-\alpha$ of atom layer n will remain uncovered. The effective model interaction for an average thickness $t=(n+\alpha)d$ is simply

$$J_m(t) = (1-\alpha)J_m(n) + \alpha J_m(n+1), \quad (5)$$

which, normalized to $J^*=J_m$ at one monolayer, is shown as the line connecting the solid circles plotted at the bottom of Fig. 6(c). The model magnetization profile, the dashed line in Fig. 6(c), is obtained by setting all positive values of the model coupling function $J_m(t)$ to the same positive magnetization value, and all negative values to a negative magnetization of the same magnitude, plotted as $M/M^*=+1$ or -1 , respectively. The relative magnetization measured by SEMPA is normalized to the saturation value M^* in a range of Cr thickness from 20 to 30 monolayers. In the region where the Cr spacer layer is very thin, the measured M/M^* becomes greater than 1 by an amount depending on the Fe overlayer thickness, owing to the contribution of secondary electrons from the Fe whisker. The exact coupling periods and uncertainties

are determined by varying the periods L_A and L_B , and searching for the best match between the calculated and measured magnetization profiles. Each time the periods are varied, the amplitudes and phases are adjusted to optimize the fit. The result shown in Fig. 6(c) for Cr growth at 350°C had the following parameters: $A=1$, $L_A=2.105\pm 0.005d$, $\Phi_A=3.82$, $B=0.8$, $L_B=12.0\pm 1d$, and $\Phi_B=0.6$. The high accuracy to which the short-period oscillation can be determined is a result of the accurate thickness determination from the RHEED intensity oscillations (± 0.1 monolayer), and the large number of periods over which the exchange coupling oscillations persist.

The magnetization calculated from the model interaction of Eq. (4) with the above parameters is seen to fit the measured magnetization of Fig. 6(c) even for small Cr thicknesses, where it is not necessary to assume any extrinsic effect such as pinholes as a driving force for the ferromagnetic coupling. The t^{-1} Cr thickness dependence of the short-period coupling provides a fit that is somewhat better than obtained with a t^{-2} thickness dependence; it is qualitatively comparable to the fit obtained with a t^0 Cr thickness dependence suggested for the short period for antiferromagnetic Cr.²² Since SEMPA does not measure the strength of the coupling, other measurements, such as magneto-optic Kerr measurements of the magnetic-field dependence of the coupling, will be necessary to determine the thickness dependence of the coupling.

The very accurate determination of the short period of the coupling provided by SEMPA allows us to rule out a recent suggestion²³ that a ‘‘Vernier’’ period of the first harmonic of the short period oscillation is the origin of the long-period coupling. The first harmonic is of the form $\sin(2\pi mnd/L_A + \Phi'_A)$ with $m=2$, which leads to a Vernier period of the first harmonic, $L'_A=L_Ad/(L_A-2d)$. The Vernier period of the first harmonic of the measured short-period oscillation is thus found to be $L'_A=20.05d$, compared to the experimental value of $12\pm 1d$ from the SEMPA measurements. There is a range of Fermi-surface spanning vectors associated with the short-period coupling, but calculations show that even the shortest of these gives a Vernier period of $14.23d$.²⁴ For a Vernier period to be the origin of the measured long period, $12d$, the short period would have to be $L_A=2.182d$, which is 15 standard deviations off the experimentally determined value of $2.105\pm 0.005d$.

V. EFFECT OF ROUGHNESS OF COUPLING

The origin of the very strong dependence of the SEMPA magnetization images on the growth temperature of the Cr spacer layer is expected to be associated with variations in the roughness of the Cr growth. In addition to the rms height fluctuation, roughness is characterized by a lateral correlation length for fluctuations that is related to the island size distribution, seen in Fig. 4 to vary widely. Also, unlike our experimental situation where the interface with the Fe whisker is smooth, in general, the amount of mutual correlation of the two interfaces of the spacer layer must be taken into account

when considering the effect of roughness on the coupling.

There are two ways that the roughness is expected to influence the interlayer coupling:^{20,21} (1) the coupling must be averaged over thickness fluctuations in the film, and (2) the coupling strength can be affected by the breaking of in-plane translational invariance and thus parallel momentum conservation at the interface. Wang, Levy, and Fry²⁵ considered the first of these effects to explain the absence of the short-period oscillations, predicted by their calculations of the exchange coupling in Fe/Cr/Fe, in experiments available at that time. We show that the magnetization images can be explained by the averaging of the coupling due to the thickness fluctuations associated with the roughness of the lower-temperature Cr growth as determined by STM measurements. It is not necessary to include roughness-dependent changes in the coupling $J(n)$.

Unlike the case for layer-by-layer growth, for a film with thickness fluctuations, even if it has an average thickness of exactly n monolayers, there may be thicknesses of $n-2$, $n-1$, n , $n+1$, and $n+2$ monolayers present in the growth front, as is the case for example in Fig. 4(a). In an extension of Eq. (5), which we used for layer-by-layer growth, we can calculate the model interaction at any thickness $J_m(t)$ by adding the contributions of $J_m(n)$ of each layer of thickness nd weighted by the fractional area of that layer thickness in the interface. If we assume a Gaussian interface width σ , smoothly varying with thickness according to Eq. (2), the fraction of each layer of thickness nd in the interface of a film of thickness t is

$$P(t, n) = [(2\pi)^{1/2}\sigma(t)]^{-1} \exp\left\{-\left[(t - nd)/\sigma(t)\right]^2/2\right\}, \quad (6)$$

and the model interaction is

$$J_m(t) = \sum_n P(t, n) J_m(n). \quad (7)$$

This interaction is plotted at the bottom of Fig. 6(a) using the σ from the STM image for Cr growth at 50 °C and assuming a $\beta=0.457$. Remains of the short-period oscillations are not apparent in $J_m(t)$ beyond about ten monolayers. Note, however, that the $J_m(t)$ which is plotted is determined from $J_m(n)$, which has the same parameters determined from the high-temperature layer-by-layer growth. The SEMPA magnetization profile calculated from this model interaction reproduces the data reasonably well, although it fails to reproduce the residual short-period fine structure at six monolayers. The roughness introduced by Wang, Levy, and Fry²⁵ to eliminate the short-period oscillations they calculated is in the same spirit as Eqs. (6) and (7). They assumed a simpler, constant roughness given by a three-layer growth model in which a quarter of the interface atoms are shifted by one monolayer.

The magnetization profile shown in Fig. 6(b) for growth at the intermediate temperature shows remnants of short-period oscillations up to thicknesses of about 18 layers. Using Eqs. (6) and (7) and σ determined from the STM image of Fig. 4(b) with the same $\beta=0.457$, one obtains $J_m(t)$ plotted at the bottom of Fig. 6(b). The calcu-

lated magnetization profile shows an additional oscillation not present in the experimental data at a Cr thickness of 23 monolayers; a close examination of $J_m(t)$ at the bottom of Fig. 6(b) shows that it barely crosses zero at that point, and hence it would be very sensitive to a slight difference in the value used for the roughness. In the thinner region of the Cr spacer layer, the experimental magnetization profiles of Figs. 6(b) and 6(c) exhibit incomplete short-period magnetization reversals even though there are complete reversals in the calculated magnetizations. The partial reversals can be understood in terms of an additional coupling—the biquadratic coupling—as discussed below.

Although the differences in the magnetization images so sharply illustrated in Fig. 2 are sometimes attributed to interface roughness, our measurements and analysis above show that it is really the fluctuations in the Cr spacer-layer thickness that are important. Even on a very smooth Fe whisker, there are approximately ten steps in the whisker surface over the 10 μm it takes for the Cr film to increase by one monolayer. In layer-by-layer growth, the step is just replicated in the top surface of the Cr layer. In principle then, a smooth substrate like an Fe whisker is not needed to observe the short-period oscillations. However, substrate roughness may hinder good layer-by-layer growth, leading to thickness fluctuations which prevent observation of short-period oscillations.

VI. CHARACTERISTIC LENGTHS

There are characteristic lengths important to understanding the exchange-coupling interaction and our experimental results. Knowledge of these length scales helps understand why, for a Cr film like that in the STM image of Fig. 4(c), the magnetization of an Fe overlayer does not locally align in the direction determined by $J(n)$ for the underlying number of Cr monolayers. Since the island edges visible in the STM images are abrupt steps, there would be regions of Fe aligned in one direction determined by $J(n)$ bordering regions aligned in the opposite direction determined by $J(n-1)$. Such an alignment would be at a large cost in intralayer exchange energy of the Fe overlayer along the boundary. It is for this reason that in bulk Fe the magnetization direction changes from one domain to another gradually over some distance, or domain-wall width, of order 100 nm. The domain-wall width is determined by a balance between the intralayer exchange, characterized by the exchange stiffness A_{ex} , which works to prevent an abrupt change in magnetization, and the anisotropy which limits the width of the wall.

Similarly, in the Fe overlayer of our experiment, there is a transition distance ℓ_{wall} over which the magnetization reverses direction, which in principle could be obtained from a micromagnetic calculation. Ribas and Dieny²⁶ pointed out that in calculating ℓ_{wall} , J_1 plays a role like the anisotropy in a bulk domain-wall calculation; that is, it works to limit the width of the transition region. In their two-dimensional calculation for Fe films of equal thickness, they found that ℓ_{wall} set the minimum

terrace length for there to be complete magnetic alignment near the terrace center. In the Fe/Cr/Fe system, the three-dimensional Cr islands of thickness nd must have a minimum size in order for the Fe overlayer to align according to $J_1(n)$. This minimum size can be characterized for a circular region by a diameter δ .

There is no micromagnetic calculation of ℓ_{wall} or δ for our experimental geometry, but some limits can be inferred from the STM and SEMPA measurements. The characteristic size of the exposed "islands" of thickness n and $n+1$ monolayers reaches a maximum estimated from Fig. 4(c) to be approximately 50 nm. There is no evidence from the SEMPA measurements that the magnetization in the Fe overlayer is breaking up into small magnetic regions corresponding to this island size; this would be manifested by the measurement of a reduced magnetization owing to the averaging of oppositely aligned magnetization regions within the SEMPA probe size, which was 100 nm for the measurements of Fig. 2 (and 6). Thus the critical dimension δ for the island to have its own magnetization is greater than 50 nm. In analogy with the two-dimensional case,²⁶ ℓ_{wall} may be similar in size to δ . This justifies our assumption throughout the discussion of the previous sections that the critical dimension δ is larger than the islands in the Cr growth front, so that the effective exchange $J_1(t)$ is a weighted average of the contributing coupling strengths $J_1(n)$.

In the other extreme, we have assumed that δ is much smaller than the distance over which there is a significant change of average thickness in the Cr wedge. Thus if two magnetic regions are separated by a distance much greater than the minimum size for a region to establish its own magnetization direction, they behave independently. Since the Cr film increases in thickness by an atomic layer approximately every ten micrometers, regions of average Cr thickness differing by one monolayer are magnetically well separated. This is the reason that the exchange coupling of magnetic layers can be studied with a wedge-shaped spacer layer of linearly increasing thickness without a region of one thickness interfering with another. We have varied the wedge angle outside the range of angles typically used in order to be sure that there are no effects of one region interfering magnetically with another.

VII. BIQUADRATIC COUPLING

The SEMPA magnetization profiles of Fig. 6 show that, especially at smaller Cr thicknesses, the magnetization does not switch completely from being along the direction of the wedge to being antiparallel to it. The magnitude of the magnetization is not decreased; rather, there is another component of the magnetization in the plane of the Fe film, transverse to the wedge direction. To understand the origin of this effect, which was observed in early Kerr effect²⁷ and SEMPA (Ref. 8) studies of the exchange coupling in Fe/Cr/Fe structures, we must look beyond the bilinear coupling J_1 of Eq. (3). A phenomenological expression for the exchange energy E_s per unit area of the spacer layer surface can be written²⁸

$$E_s = -J_1 \cos \psi - J_2 \cos^2 \psi, \quad (8)$$

where ψ is the angle between the magnetization of the two Fe layers. In addition to the first, or bilinear coupling, term in Eq. (8), there is a second term which represents the biquadratic coupling J_2 . The biquadratic coupling could be either of intrinsic origin, as discussed by Erickson, Hathaway, and Callen,²⁹ or of extrinsic origin as proposed by Slonczewski.³⁰ Equation (8) has the interesting property that when J_2 is negative the energy is minimized when the magnetizations of the two magnetic layers move from colinear toward perpendicular alignment.

In the theory of Slonczewski, the growth of the Cr layer influences not only the bilinear coupling but also the biquadratic coupling, the origin of which is attributed to fluctuations in the bilinear coupling caused by fluctuations in the thickness of the spacer layer.³⁰ The intralayer exchange coupling in the Fe overlayer hinders magnetization reversals over microscopic spatial dimensions, as would be dictated by the fluctuations in the bilinear coupling, and the energy is lowered by the magnetic moments turning toward a direction perpendicular to the competing bilinear coupling directions. By rotating perpendicular to the substrate magnetization, the upper film can take advantage of the energy gain associated with rapidly varying but small fluctuations in the magnetization direction. When the Fe overlayer thickness D is small compared to the characteristic length scale Λ of the islands which give the thickness fluctuations, the leading contribution to the biquadratic term in Slonczewski's model goes as

$$J_2 \propto -(\Delta J)^2 \Lambda^2 / A_{\text{ex}} D, \quad (9)$$

where A_{ex} is again the intralayer exchange coupling. The fluctuation in the bilinear coupling ΔJ is just the difference in J_1 over the thickness fluctuation. Thus biquadratic coupling is expected whenever there are thickness fluctuations coupled with a variation of the bilinear coupling with thickness, regardless of the period of the bilinear coupling. The coupling is dominated by the bilinear coupling, except at thicknesses where the bilinear coupling changes sign; it is in these regions that biquadratic coupling is observed with SEMPA. However, it is possible to determine the biquadratic and bilinear coupling independently over the whole Cr thickness range with Brillouin light scattering, as shown in measurements of Fe/Cr/Fe(100) whisker systems for which the layer-by-layer growth was optimized with RHEED measurements.³¹

The biquadratic coupling is manifested in the SEMPA measurements in two ways. First, because the total coupling is dominated by the bilinear term, the biquadratic coupling is observed at Cr thicknesses where there is a transition from ferromagnetic to antiferromagnetic coupling and the average bilinear coupling goes through zero. In this transition region the biquadratic term is larger, and the magnetic domains in the Fe overlayer are at 90° to the domains in the Fe whisker. We have observed⁸ biquadratic coupling of the Fe overlayer in SEMPA images of the in-plane magnetization component M_x

that is orthogonal to that imaged in Fig. 1. The width of a region in which biquadratic coupling is observed corresponds to a particular range of average Cr thickness.

Second, the biquadratic coupling is observed in the SEMPA M_y magnetization profiles (see Fig. 6) as a reduction in M_y at the thinner part of the Cr wedge. A reduction in this component of the magnetization is accompanied by an increase in M_x . Thus the magnetization of the Fe overlayer rotates with respect to the substrate magnetization in this thickness region, and does not completely switch from parallel to antiparallel coupling. In the extrinsic model of Slonczewski,³⁰ there must be the short-period bilinear coupling present [apparent in $J_m(t)$, Fig. 6] for this short-period biquadratic effect to occur. The partial rotation caused by biquadratic coupling is not observed at larger thicknesses. This is consistent with Eqs. (3) and (9), which show that the $1/t$ dependence of the bilinear coupling becomes a $(1/t^2)$ dependence for the biquadratic coupling, which rapidly becomes less important with increasing thickness. [The biquadratic coupling observed by SEMPA at large interlayer thicknesses in Fe/Ag/Fe(100) structures³² may be the result of an alternate mechanism connected with the magnetic dipole field.³³] The growth is also better in thinner layers leading to larger islands and hence, from Eq. (9), a larger biquadratic coupling in the Slonczewski picture. When the islands reach a size greater than δ , the Fe overlayer couples parallel or antiparallel to the other Fe layer, and Eq. (9) breaks down. In principle, the characteristic island size Λ is determined from the STM measurements, and one might expect to be able to estimate the relative biquadratic coupling strengths for films grown at different temperatures. However, the model³⁰ would need to be extended to apply to more general thickness fluctuations and island distributions before quantitative estimates are possible.

VIII. CONCLUSION

STM measurements provide a quantitative picture of the Cr growth at each substrate temperature. The layer-

by-layer growth at 300°C observed in the STM images explains why the short-period oscillations of the exchange coupling can be observed in the SEMPA magnetization images. We showed how the periods of oscillation of a theoretical coupling function could be obtained by fitting to the SEMPA magnetization profile in the case of layer-by-layer growth. For growth at lower temperatures, the fractional exposure of the several thicknesses present in the growth front was found to be fit well by a Gaussian. Assuming the exchange coupling at each island of Cr of thickness nd to be the same as the exchange coupling for the same thickness in layer-by-layer growth, we were able to obtain good agreement with the measured magnetization profile at lower Cr growth temperatures by adding the weighted contribution to the coupling from each Cr layer thickness contributing to the average thickness. Other consequences of roughness at the interface, such as the breakdown of translational invariance, are not required to explain the data.

It is clear from the STM and SEMPA results that a growth parameter, in this case the Fe whisker substrate temperature, which leads to different modes of growth strongly influences the exchange coupling of the magnetic layers. Thus knowledge of the physical structure is crucial to understanding the magnetic properties of a material.

ACKNOWLEDGMENTS

We wish to thank M. D. Stiles for helpful discussions, and R. A. Dragoset for his assistance in this project. This work was supported by the Office of Technology Administration of the Department of Commerce and by the Office of Naval Research. The whiskers were grown at Simon Fraser University under an operating grant from the National Science and Engineering Research Council of Canada.

¹M. N. Baibich, J. M. Broto, A. Fert, F. Nguyen Van Dau, F. Petroff, P. Etienne, G. Creuzet, A. Friederich, and J. Chazelas, *Phys. Rev. Lett.* **61**, 2472 (1988).

²G. Binasch, P. Grünberg, F. Saurenbach, and W. Zinn, *Phys. Rev. B* **39**, 4828 (1989).

³P. Grünberg, R. Schreiber, Y. Pang, M. B. Brodsky, and H. Sowers, *Phys. Rev. Lett.* **57**, 2442 (1986).

⁴In this field the terms "layers" and "films" are often used interchangeably. Although "layer" is often used to refer to a single atomic layer, we will try to avoid confusion by using "monolayer" or "atomic layer" when referring to units of a single atomic layer thickness. The terms "interlayer" and "spacer layer" are sometimes used interchangeably for the nonferromagnetic spacer layer. We reserve the term "interlayer" for use in a different sense, that is, when speaking of the interlayer coupling between two ferromagnetic films. Note that experimental uncertainties quoted in this paper are

one standard deviation.

⁵S. S. P. Parkin, N. More, and K. P. Roche, *Phys. Rev. Lett.* **64**, 2304 (1990).

⁶See, for example, the compilation of experimental results in Ref. 20.

⁷K. B. Hathaway, in *Ultrathin Magnetic Structures II*, edited by B. Heinrich and J. A. C. Bland (Springer-Verlag, Berlin, in press).

⁸J. Unguris, R. J. Celotta, and D. T. Pierce, *Phys. Rev. Lett.* **67**, 140 (1991).

⁹J. Unguris, R. J. Celotta, and D. T. Pierce, *Phys. Rev. Lett.* **69**, 1125 (1992).

¹⁰J. Unguris, D. T. Pierce, R. J. Celotta, and J. A. Strosio, in *Magnetism and Structure in Systems of Reduced Dimension*, edited by R. F. C. Farrow *et al.* (Plenum, New York, 1993).

¹¹J. Unguris, M. R. Scheinfein, R. J. Celotta, and D. T. Pierce, in *Chemistry and Physics of Solid Surfaces VIII*, edited by R.

- Vanselow and R. Howe (Springer, Berlin, 1990), p. 239.
- ¹²M. R. Scheinfein, J. Unguris, M. H. Kelley, D. T. Pierce, and R. J. Celotta, *Rev. Sci. Instrum.* **61**, 2501 (1990).
- ¹³J. A. Stroscio and D. T. Pierce, *J. Vac. Sci. Technol.* (to be published).
- ¹⁴A. S. Arrott, B. Heinrich, and S. T. Purcell, in *Kinetics of Ordering and Growth at Surfaces*, edited by M. G. Lagally (Plenum, New York, 1990), p. 321.
- ¹⁵P. N. First, J. A. Stroscio, D. T. Pierce, R. A. Dragoset, and R. J. Celotta, *J. Vac. Sci. Technol. B* **9**, 531 (1991); J. A. Stroscio, D. T. Pierce, R. A. Dragoset, and P. N. First, *ibid. A* **10**, 1981 (1992).
- ¹⁶J. A. Stroscio, D. T. Pierce, J. Unguris, and R. J. Celotta, *J. Vac. Sci. Technol.* (to be published).
- ¹⁷Y.-W. Mo, J. Kleiner, M. B. Webb, and M. G. Lagally, *Phys. Rev. Lett.* **66**, 1998 (1991); *Surf. Sci.* **268**, 275 (1992).
- ¹⁸J. A. Stroscio, D. T. Pierce, and R. A. Dragoset, *Phys. Rev. Lett.* **70**, 3615 (1993).
- ¹⁹Y.-L. He, H.-N. Yang, T.-M. Lu, and G.-C. Wang, *Phys. Rev. Lett.* **69**, 3770 (1992).
- ²⁰M. D. Stiles, *Phys. Rev. B* **48**, 7238 (1993).
- ²¹P. Bruno and C. Chappert, *Phys. Rev. B* **46**, 261 (1992).
- ²²M. van Schilfgaarde and F. Herman, *Phys. Rev. Lett.* **71**, 1923 (1993).
- ²³M. van Schilfgaarde and W. A. Harrison, *Phys. Rev. Lett.* **71**, 3870 (1993).
- ²⁴M. D. Stiles (private communication).
- ²⁵Y. Wang, P. M. Levy, and J. L. Fry, *Phys. Rev. Lett.* **65**, 2732 (1990).
- ²⁶R. Ribas and B. Dieny, *Phys. Lett. A* **167**, 103 (1992).
- ²⁷M. Rührig, R. Schäfer, A. Hubert, R. Mosler, J. A. Wolf, S. Demokritov, and P. Grünberg, *Phys. Status Solidi A* **125**, 635 (1991).
- ²⁸P. A. Grünberg, A. Fuss, Q. Leng, R. Schreiber, and J. A. Wolf, in *Magnetism and Structure in Systems of Reduced Dimension* (Ref. 10).
- ²⁹R. P. Erickson, K. B. Hathaway, and J. R. Cullen, *Phys. Rev. B* **47**, 2626 (1993).
- ³⁰J. C. Slonczewski, *Phys. Rev. Lett.* **67**, 3172 (1991).
- ³¹B. Heinrich, M. From, J. F. Cochran, L. X. Liao, Z. Celinski, C. M. Schneider, and K. Myrtle, in *Magnetic Ultrathin Films*, edited by B. T. Jonker *et al.*, MRS Symposia Proceedings No. 313 (Materials Research Society, Pittsburgh, 1993), p. 119.
- ³²J. Unguris, R. J. Celotta, and D. T. Pierce, *J. Magn. Magn. Mater.* **127**, 205 (1993).
- ³³S. Demokritov, E. Tsybal, P. Grünberg, W. Zinn, and I. Schuller, *Phys. Rev. B* **49**, 720 (1994).

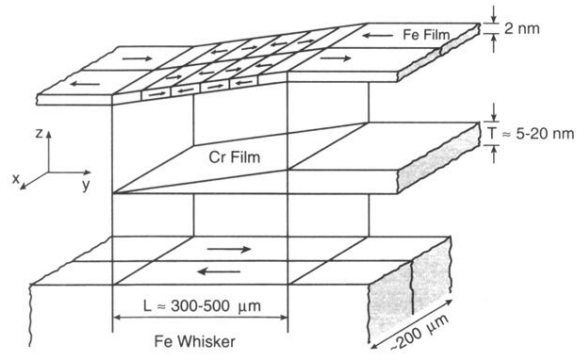


FIG. 1. A schematic exploded view of the Fe/Cr/Fe(100) sample structure showing the Fe(100) single-crystal whisker substrate, the Cr wedge, and the Fe overlayer. The arrows show the magnetization direction in each domain. The z scale is expanded approximately 5000 times.

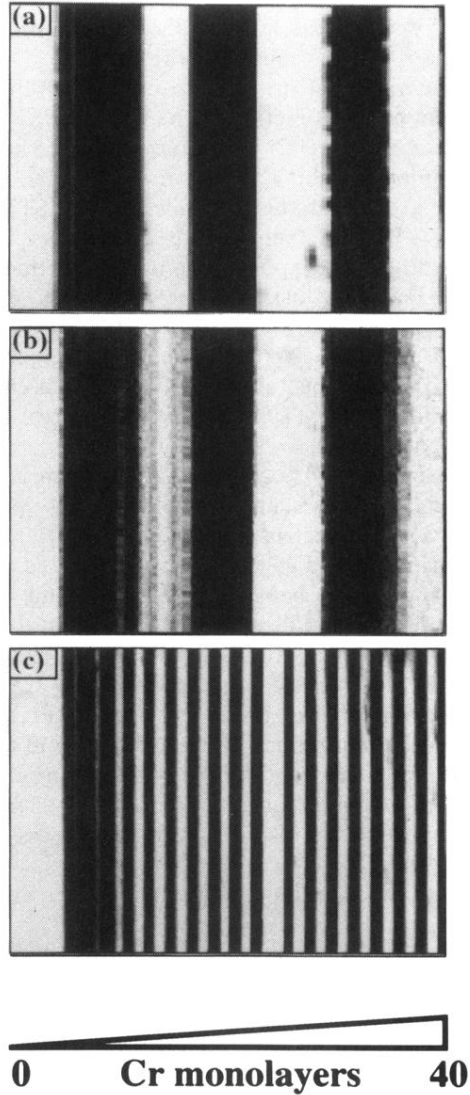


FIG. 2. SEMPA magnetization images of the Fe overlayer coupled through Cr spacer layers grown at Fe substrate temperatures of (a) 30, (b) 200, and (c) 350 °C, respectively. The Cr spacer layer increases in thickness from 0 to 40 monolayers, as indicated, from the left to the right of the images. The magnetization of the Fe overlayer is parallel (ferromagnetically coupled) to the substrate in the white regions, and antiparallel (antiferromagnetically coupled) in the black regions.

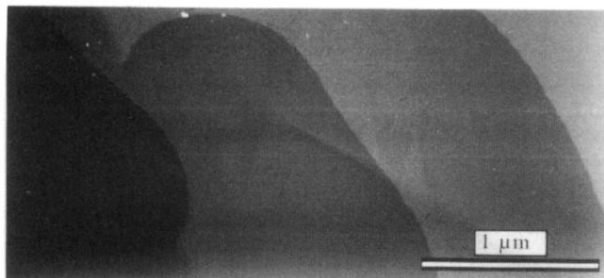


FIG. 3. A $1.6 \times 3.5\text{-}\mu\text{m}$ STM image of the clean Fe(100) whisker surface showing the typical step density of approximately one per micrometer. Higher regions of the surface are indicated by lighter gray levels.

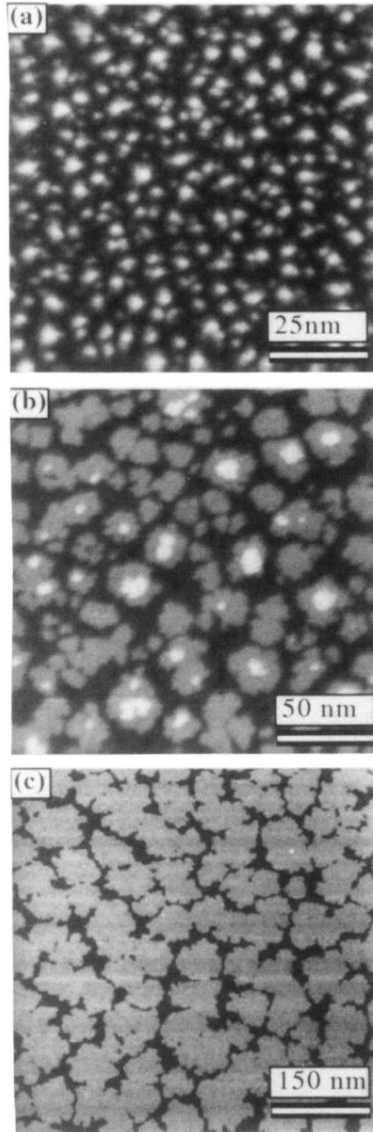


FIG. 4. STM images show the growth of Cr on the Fe(100) whisker substrate held at (a) 50, (b) 215, and (c) 300 °C. The images are 100×100 , 200×200 , and 600×600 nm, respectively.